ELSEVIER

Optics and Lasers in Engineering 33 (2000) 49–64

OPTICS and LASERS in ENGINEERING

Integrated photoelasticity for nondestructive residual stress measurement in glass

H. Aben*, L. Ainola, J. Anton

Laboratory of Photoelasticity, Institute of Cybernetics, Tallinn Technical University, Akadeemia tee 21, 12618 Tallinn, Estonia

Received 30 November 1999; accepted 4 February 2000

Abstract

The paper gives a review of integrated photoelasticity and of its application for residual stress measurement in glass. By considering the basic theory of the method, two particular cases, the case of weak birefringence and that of constant principal stress axes, are picked up. It is shown that integrated photoelasticity is actually optical tensor field tomography. Its peculiarities in comparison with scalar field tomography are considered. Since directly integrated photoelasticity allows for the measurement of only some of the stress components, analytical or numerical methods are to be used for complete determination of the stress field. Nonlinear optical phenomena, interference blots and fringe bifurcation, are briefly considered. Several examples illustrate the application of the method.

Keywords: Photoelasticity; Residual stress; Glass; Nondestructive testing

1. Introduction

Residual stress is one of the most important characteristics of glass articles from the point of view of their strength and resistance [1,2]. In the case of optical glass, birefringence caused by the residual stresses characterizes the optical quality of the article.

During about a century, photoelasticity [3] has been the most widely used method for quality control in the glass industry. Two-dimensional photoelasticity permits the determination of the so-called form stresses (which are constant through the thickness in flat glass). As for the thickness stresses (which vary parabolically through the

* Corresponding author. Tel. + 372-6204180; fax + 372-6204151.
E-mail address: aben@ioc.ee (H. Aben).

0143-8166/00/$ - see front matter
PII: S0143-8166(00)00018-X

thickness), their distribution can be determined using the scattered light method. Specific methods have been developed for nondestructive determination of the stresses on the surfaces of the flat glass [4].

It is much more complicated to estimate stresses in glass articles of complicated shape: in bottles, drinking glasses, tubes, fibres and fibre preforms, etc. At the same time, development of glass technology demands exact information about the residual stresses in glass articles. Let us mention that while numerical methods are being successfully used for the calculation of stresses in glass caused by external loads (e.g., by internal pressure in bottles [5,6]), their application for the calculation of the residual stresses gives less reliable results due to the lack of exact data about the temperature distribution and physical parameters of the specimen during various phases of the production process [7].

Thus, development of experimental, desirably nondestructive, methods for residual stress measurement in glass articles of complicated shape is of current interest. For this purpose during the last two decades considerable development of integrated photoelasticity has taken place. In this paper, basic theory, measurement technology, and several applications of integrated photoelasticity in glass stress measurement are described.

2. Integrated photoelasticity

In integrated photoelasticity [4,8], the three-dimensional transparent specimen is placed in an immersion tank and a beam of polarized light is passed through the specimen (Fig. 1). Transformation of the polarization of light is measured for many light rays, and, except the case when the specimen is axisymmetric, for many azimuths of the light beam. In certain cases, distribution of some (or all) stress components can be determined using the integrated measurement data.

Propagation of polarized light in the direction of the z-axis through a 3-D inhomogeneous birefringent medium is governed by the following equations [8]:

$$\frac{\mathrm{d}E_x}{\mathrm{d}z} = -\frac{1}{2}\mathrm{i}C(\sigma_x - \sigma_y)E_x - \mathrm{i}C\tau_{xy}E_y,$$

$$\frac{\mathrm{d}E_y}{\mathrm{d}z} = -\mathrm{i}C\tau_{xy}E_x + \frac{1}{2}\mathrm{i}C(\sigma_x - \sigma_y)Ey, \tag{1}$$

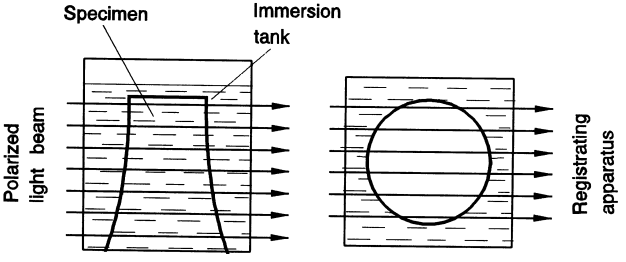

Fig. 1. Experimental set-up in integrated photoelasticity.

where E_x and E_y are components of the electric vector along the axes x and y, C is the photoelastic constant, and σ_x,σ_y and τ_{xy} are components of the stress tensor in the plane xy.

Solution of Eqs. (1) can be expressed as [8]

$$\begin{pmatrix} E_{x*} \\ E_{y*} \end{pmatrix} = U \begin{pmatrix} E_{x0} \\ E_{y0} \end{pmatrix}, \tag{2}$$

where E_{x0} and E_{y0} are components of the incident light vector, E_{x*} and E_{y*} are those of the emergent light vector, and U is a 2×2 unitary unimodular matrix.

Analysis of the transformation matrix U has shown that there always exist two mutually perpendicular directions of the polarizer by which the light emerging from the specimen is linearly polarized. These directions of polarization of the incident and emergent light are named the primary and secondary characteristic directions. Due to their exceptional physical properties, characteristic directions can be determined experimentally. Besides these, it is possible to measure the characteristic optical retardation.

In the general form the inverse problem of integrated photoelasticity may be formulated as follows. Stress field of the specimen can be described as a set of functions which contain a number of unknown coefficients. Photoelastic measurements are to be carried out for many light rays in many directions. Parameters of the transformation matrix U for every ray depend on the stress coefficients. The latter are to be determined on the basis of the characteristic parameters. In addition, equations of the theory of elasticity are to be used. Thus, in the general case the inverse problem of integrated photoelasticity is highly complicated.

3. Two particular cases

System (1) can be written in the matrix form as

$$\frac{\mathrm{d}E}{\mathrm{d}z} = AE, \tag{3}$$

where

$$E = \begin{pmatrix} E_x \\ E_y \end{pmatrix}, \tag{4}$$

$$A = -\frac{1}{2}\mathrm{i}C \begin{pmatrix} \sigma_x - \sigma_y & 2\tau_{xy} \\ 2\tau_{xy} & -(\sigma_x - \sigma_y) \end{pmatrix}. \tag{5}$$

Using the Peano–Baker method, the solution of Eq. (3) can be written, following Eq. (2), in the form

$$U = I + \int_0^z A\,\mathrm{d}z + \int_0^z A\left(\int_0^z A\,\mathrm{d}z\right)\mathrm{d}z + \cdots. \tag{6}$$

In zero approximation $U = I$. That is the case when the medium is not birefringent ($C = 0$). First approximation [the first two terms in Eq. (6)] reveals

$$U = \begin{pmatrix} 1 - \frac{1}{2}(\frac{\Delta}{2})^2 + \mathrm{i}\frac{\Delta}{2}\cos 2\varphi & \mathrm{i}\frac{\Delta}{2}\sin 2\varphi \\ \mathrm{i}\frac{\Delta}{2}\sin 2\varphi & 1 - \frac{1}{2}(\frac{\Delta}{2})^2 - \mathrm{i}\frac{\Delta}{2}\cos 2\varphi \end{pmatrix}, \tag{7}$$

where

$$\Delta = C\int_0^z (\sigma_1 - \sigma_2)\,\mathrm{d}z, \tag{8}$$

$$\tan 2\varphi = \frac{2\int \tau_{xy}\,\mathrm{d}z}{\int(\sigma_x - \sigma_y)\,\mathrm{d}z}. \tag{9}$$

Matrix U is the matrix of a birefringent plate with weak birefringence:

$$\sin\frac{\Delta}{2} \cong \frac{\Delta}{2}, \tag{10}$$

$$\cos\frac{\Delta}{2} \cong 1 - \frac{1}{2}\left(\frac{\Delta}{2}\right)^2. \tag{11}$$

It follows that in the case of weak birefringence, a 3-D photoelastic model behaves optically similarly to a single birefringent plate. It is possible to measure the parameter of the isoclinic φ and optical retardation Δ, which are related to the components of the stress on the light ray through the relationships

$$V_1 = \Delta\cos 2\varphi = C\int_0^z (\sigma_x - \sigma_y)\,\mathrm{d}z, \tag{12}$$

$$V_2 = \Delta\sin 2\varphi = 2C\int_0^z \tau_{xy}\,\mathrm{d}z. \tag{13}$$

It is possible to show that if rotation of the principal stress axes on the light ray is moderate, Eqs. (12) and (13) are valid also in the case when conditions (10) and (11) are not observed. If there is no rotation of the principal stress axes, Eqs. (12) and (13) are valid for arbitrary birefringence. In this case, Eqs. (12) and (13) can be written as

$$\Delta = C\int_0^z (\sigma_1 - \sigma_2)\,\mathrm{d}z, \tag{14}$$

which is named the integral Wertheim law.

4. Integrated photoelasticity as optical tomography of the tensor field

Since determination of stress in integrated photoelasticity is in certain cases based on integral relationships (12) and (13), its analogy with tomography is evident. In tomography [9,10], for the determination of the internal structure of an object,

a certain radiation is passed through a section of the test object (Fig. 2) and a property of this radiation, after it has passed the object, is measured. This property may be intensity, phase, polarization, etc. Such measurements are made for a great number of rays and for a great number of observation directions.

Let $f(r,\varphi)$ be the function which describes the field to be determined. What is measured experimentally is the Radon transform of the field

$$\int_{-\infty}^{\infty} f(r,\varphi)\,\mathrm{d}z = g(l,\theta). \tag{15}$$

The function $f(r,\varphi)$ can be determined with the aid of the Radon inversion

$$f(r,\varphi) = \frac{1}{2\pi^2}\int_0^{\pi}\int_{-\infty}^{\infty} \frac{\partial g(l,\theta)}{\partial l}\frac{\mathrm{d}l\,\mathrm{d}\theta}{r\cos(\theta-\varphi)-l}. \tag{16}$$

In integrated photoelasticity we have instead of Eq. (15) two integral relationships (12) and (13), which carry information about the stress field under investigation. Since stress measurement in integrated photoelasticity is also carried out by sections, it may be considered as a kind of tomography which has several peculiarities in comparison with the traditional tomography.

Traditional tomography is scalar field tomography, i.e., every point of the field is characterized by a single scalar (attenuation coefficient, scalar refractive index, etc.). Since stress is a tensor, every point of a stress field is characterized by a second-rank tensor. Thus, integrated photoelasticity is actually optical tensor field tomography with many peculiarities [11,12] which are shown in Table 1.

5. Measurement of the distribution of the normal stresses

Let us consider measurement of stresses in a 3-D specimen of arbitrary shape assuming that birefringence (or rotation of the principal stress axes) is weak. Passing

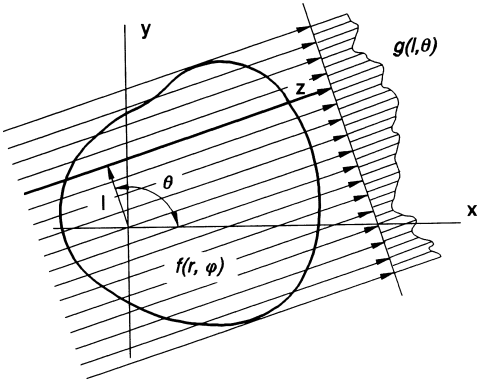

Fig. 2. In tomography experimental data $g(l,\theta)$ is recorded for many rays and many azimuths θ of the radiation.

Table 1
Scalar field vs. tensor field tomography

Scalar field tomography	Tensor field tomography
Character of the field	
Scalar $s(x, y)$	Tensor $\sigma_{ij}(x, y)$
Medium	
Mostly isotropic	Anisotropic
Radiation	
Nonpolarized	Polarized
Measurement data	
Line integrals	Nonlinear relationships, in exceptional cases line integrals
Influence of a point on the measurement data	
Does not depend on the direction of the radiation	Depends on the direction of the radiation
Preliminary information about the field	
Usually not needed	Equations of continuum mechanics
Uniqueness of the reconstructed field	
Has been proved	?

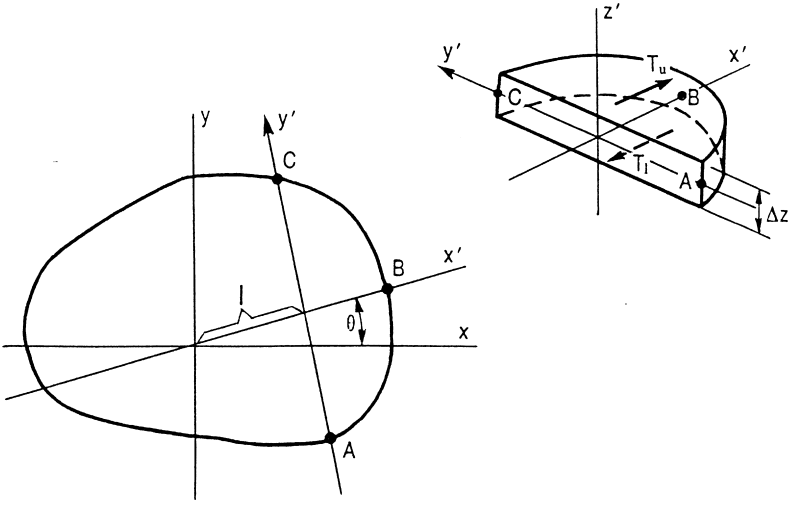

Fig. 3. Illustration to the investigation of the general 3-D state of stress.

light through the cross-section $z = \text{const}$ (Fig. 3), for each ray $y'(l,\theta)$ it is possible to measure the parameter of the isoclinic φ and optical retardation Δ.

Further, let us consider equilibrium condition for the direction x' of a 3-D segment ABC cut out of the specimen by the planes $z = z_0$, $z = z_0 + \Delta z$, and $y'z'$ (Fig. 3). The shear force in the direction of x' at the upper surface of the segment can be

expressed as

$$T_u = \int_l^B \left(\int \bar{\tau}_{zx'} \, dy' \right) dx' = \frac{1}{2C} \int_l^B \bar{V}_2 \, dx', \tag{17}$$

and at the lower surface

$$T_l = \int_l^B \left(\int \tau_{zx'} \, dy' \right) dx' = \frac{1}{2C} \int_l^B V_2 \, dx'. \tag{18}$$

Here the bar denotes values for the upper surface.

The equilibrium condition for the segment ABC in the direction of x' reveals

$$\Delta z \int_A^C \sigma_{x'} \, dy' = T_u - T_l. \tag{19}$$

From Eqs. (12) and (19) we obtain

$$\int_A^C \sigma_z \, dy' = \frac{1}{2C\Delta z} \left(\int_l^B \bar{V}_2 \, dx' - \int_l^B V_2 \, dx' \right) - \frac{V_1}{C}. \tag{20}$$

This relationship shows that from experimental data it is possible to calculate integrals of σ_z for any direction $y'(l,\theta)$. If photoelastic measurements have been carried out for a sufficient number of angles θ (turning the specimen around the z-axis), and for each θ for a sufficient number of values of l, the distribution of σ_z can be determined using methods of traditional tomography. It means that we have reduced a complicated problem of tensor field tomography to a problem of scalar field tomography for a single component σ_z of the stress tensor.

Carrying out measurements for many values of z, distribution of σ_z in all the specimen can be determined. Since the axis z, around which the specimen is rotated during measurements, can be chosen arbitrarily, distribution of all the normal stresses in any section of the specimen can be determined.

If a specimen of prismatic form with arbitrary cross-section has no stress gradient in the direction of its axis z, then in Eq. (20) we have $V_2 = \bar{V}_2 = 0$ and the distribution of σ_z is determined on the basis of photoelastic measurements in a single section.

6. Integrated photoelasticity as hybrid mechanics

6.1. Axisymmetric stress distribution

In case of an axisymmetric specimen it is sufficient to make photoelastic measurements only by one direction of the light beam. The axial stress σ_z distribution is determined from Eq. (20), and distribution of the shear stress τ_{zr} from Eq. (13) since (Fig. 3)

$$\tau_{zx} = \tau_{zr} \cos\theta. \tag{21}$$

To determine also the other stress components, the radial stress σ_r and the circumferential stress σ_θ, equations of the theory of elasticity are to be used. Combined application of experimental and analytical or numerical methods is named hybrid mechanics.

If stresses are due to external loads, stress components σ_r and σ_θ can be determined from the equilibrium equation

$$\frac{\partial \sigma_r}{\partial r} + \frac{\sigma_r - \sigma_\theta}{r} + \frac{\partial \tau_{zr}}{\partial z} = 0, \tag{22}$$

and the compatibility equation

$$\frac{\partial}{\partial r}[\sigma_\theta - \mu(\sigma_z + \sigma_r)] - (1 + \mu)\frac{\sigma_r - \sigma_\theta}{r} = 0, \tag{23}$$

where σ_z and τ_{zr} have been determined experimentally. Such an algorithm has been elaborated by Doyle and Danyluk [13].

In case of residual stresses, the compatibility equation (23) cannot be used since the source of the residual stresses is incompatible initial deformations.

By stress measurement in glass cylinders without stress gradient in the axial direction, instead of Eq. (23) the so-called classical sum rule [14] can be used:

$$\sigma_r + \sigma_\theta = \sigma_z. \tag{24}$$

If the stress gradient in the axial direction is present, one has to use the generalized sum rule which in the first approximation is [15,16]

$$\sigma_r + \sigma_\theta = \sigma_z - 3\int_0^r \frac{\partial \tau_{zr}}{\partial z}\,\mathrm{d}r + C, \tag{25}$$

where C is the integration constant to be determined from the boundary conditions. Thus, the axisymmetric residual stress distribution can be completely determined.

By derivation of Eqs. (24) and (25) it has been assumed that residual stresses in glass may be interpreted as thermal stresses due to a certain fictitious temperature field [17,18].

6.2. The case of plane deformation

For the case of plane deformation, Puro and Kell [19] have derived the following equation in cylindrical coordinates:

$$\frac{\partial^2 F}{\partial r^2} + \frac{1}{r}\frac{\partial F}{\partial r} + \frac{1}{r^2}\frac{\partial^2 F}{\partial \theta^2} = \sigma_z - \chi \tag{26}$$

submitted to the boundary conditions

$$F(r,\theta)|_{r=R} = 0, \qquad \frac{\partial}{\partial r}F(r,\theta)|_{r=R} = 0. \tag{27}$$

Here F is the stress function, χ is an arbitrary harmonic function which can be determined from the boundary conditions, and R is the radius of the specimen.

Since the axial stress distribution is known, from Eq. (26) the stress function F can be determined and stress components are calculated as follows:

$$\sigma_r = \frac{1}{r}\frac{\partial F}{\partial r} + \frac{1}{r^2}\frac{\partial^2 F}{\partial \theta^2}, \tag{28}$$

$$\sigma_\theta = \frac{\partial^2 F}{\partial r^2}, \tag{29}$$

$$\tau_{r\theta} = \frac{1}{r^2}\frac{\partial F}{\partial \theta} - \frac{1}{r}\frac{\partial^2 F}{\partial r \partial \theta}. \tag{30}$$

The complete determination of the stresses in the case of plane deformation has been considered also in rectangular coordinates [20].

7. Experimental technique

For photoelastic measurements a computer-controlled polariscope has been designed (Fig. 4). As light source, light diodes have been used. Polarizer and the first quarter-wave plate can be turned by hand. The second quarter-wave plate and the analyser are controlled by stepper motors. Specimen in an immersion tank is placed

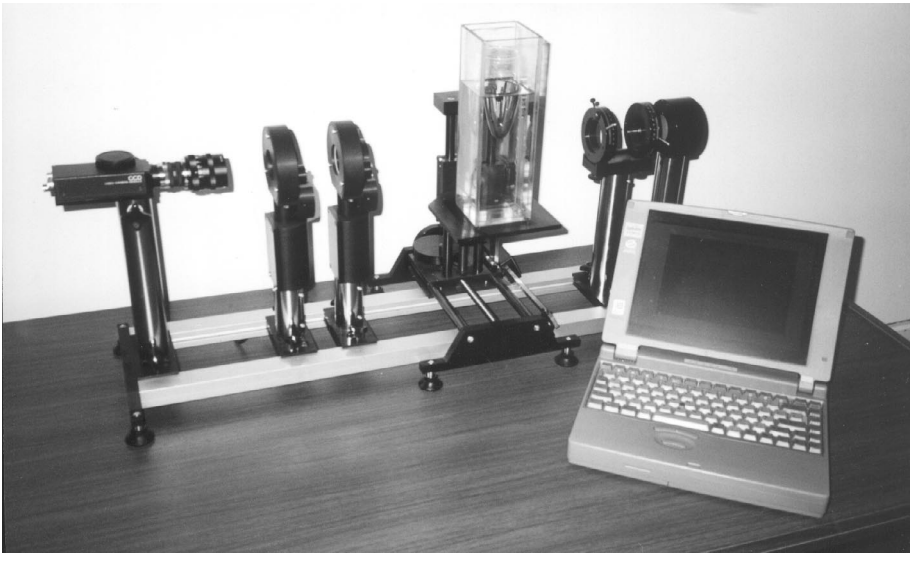

Fig. 4. Computer-controlled polariscope. In the middle is the coordinate device with the test object in the immersion tank.

on a coordinate device which enables one to select the part of the specimen to be measured.

The polariscope is supplied with software that gives the possibility to use it in several ways. First, the phase-stepping method may be used, which permits also the determination of the characteristic parameters [21]. Since in annealed glass, optical retardation is usually less than half of the wavelength and the algorithms of integrated photoelasticity demand also the azimuth of the first principal stress, a specific phase-stepping algorithm has been elaborated [22].

Second, in tempered glassware stresses can be determined using the digitized fringe pattern. In this case the main problem is automatic detection of the surfaces of the specimen and correct numbering of the fringes [23].

8. Nonlinear optical phenomena

In the basic equations of integrated photoelasticity (1) the coefficients are variable. Due to this the principle of additivity of the birefringence is not valid and the integrated fringe pattern is influenced by the distribution of birefringence as well as by the rotation of the principal stress axes. Therefore, integrated fringe patterns may have peculiarities.

Fig. 5 (left) shows the integrated fringe pattern of a diametrically loaded sphere in a light-field circular polariscope. Near the points where the load is applied, one can observe dark areas that are similar to fringes but somewhat wider and that cross the basic system of fringes. These secondary fringes are called interference blots [24].

As another example, Fig. 5 (right) shows the integrated fringe pattern of the wall-to-bottom region of a tempered drinking glass. One can observe interference blots (shown by arrows) that cross the main fringe system, bifurcation of fringes, etc.

Theoretical explanation of the appearance of the interference blots and fringe bifurcations has been given in several papers [24,25]. The main practical problem is

Fig. 5. Integrated fringe patterns in a light-field circular polariscope of a diametrically loaded sphere (left) and of the wall-to-bottom region of a tempered drinking glass (right, arrows indicate interference blots).

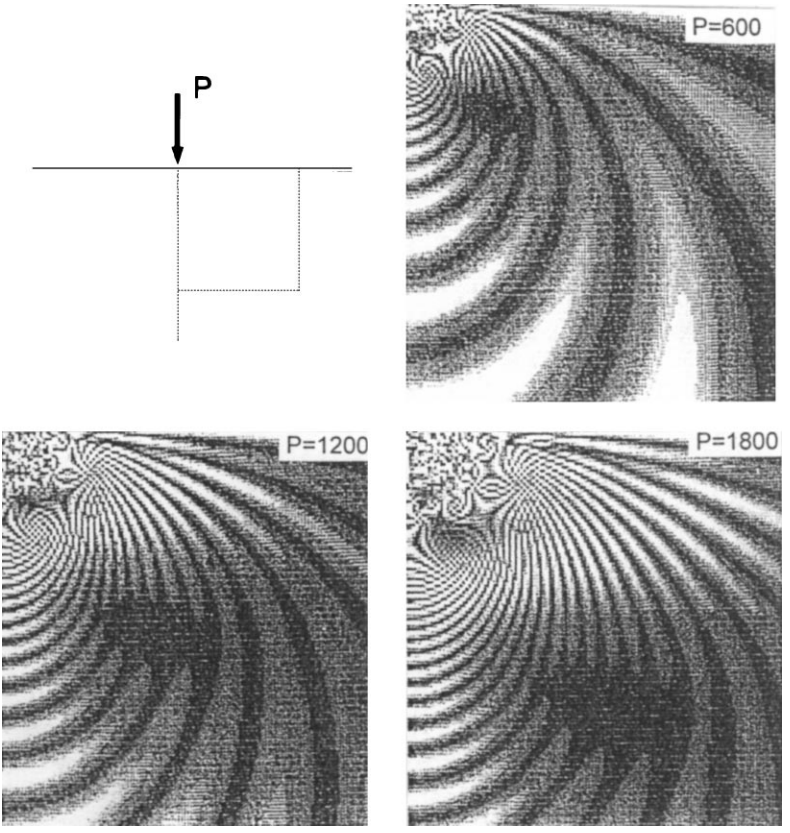

Fig. 6. Computer-generated fringe patterns for the Boussinesq problem at different loads.

the ambiguity of the fringe order which appears due to this phenomenon. In Fig. 6 computer-generated fringe patterns for the Boussinesq problem at three loads are shown. One should note that the number of fringes that emerge into the interference blot from its upper and lower parts are not equal. While the number of fringes that emerge into the interference blot from below is n, on the upper side of the blot the number of fringes is $n + 2$. Therefore, the fringe order on the left of the interference blot depends on the way the fringes are counted. This phenomenon needs further investigation.

9. Examples of application

By automatic measurement of the residual stresses in tempered glassware, the fringe pattern is shown on the screen of the computer and digitized, and using the latter stresses are calculated. Internal and external surfaces of the test object as well as dark and light fringes are automatically detected. Fig. 7 illustrates stress measurement in a tempered drinking glass. Since the stress gradient in the axial direction is weak and

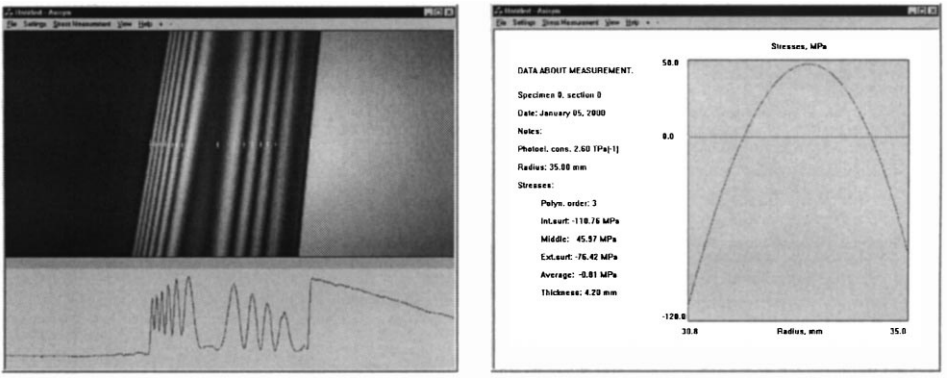

Fig. 7. Physical and digitized fringe patterns in the wall of a tempered drinking glass (left) and axial stress σ_z distribution through the wall (right).

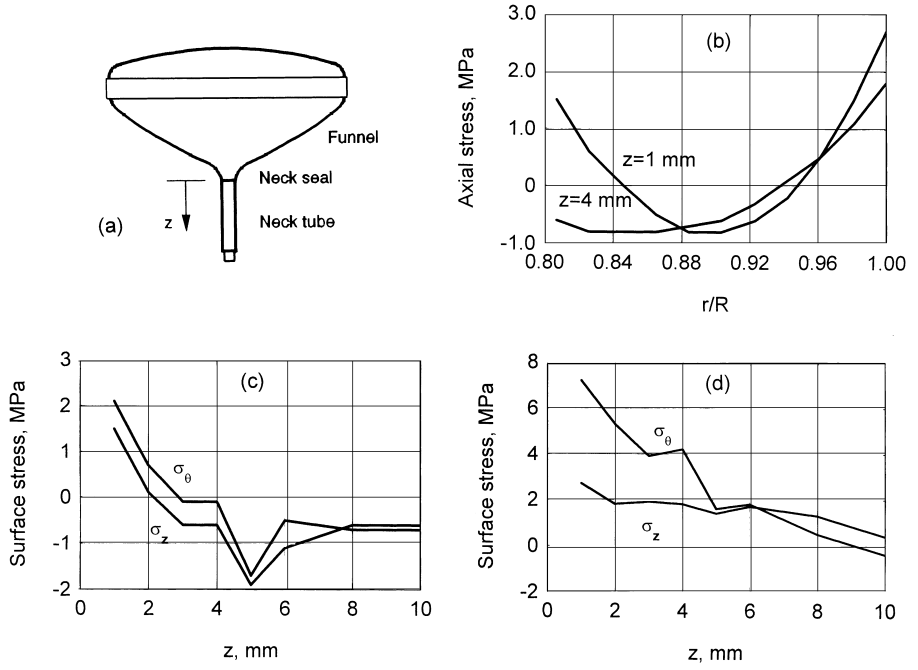

Fig. 8. Geometry of a CRT glass bulb (a), stress distribution in two sections (b), and axial and circumferential stress distribution on the internal (c) and external (d) surface of the neck tube.

$\sigma_r \cong 0$, according to the classical sum rule (24) the circumferential stress σ_θ practically equals the axial stress σ_z.

Fig. 8 shows residual stress distribution in the neck tube of a CRT glass bulb. In this case photoelastic measurements were carried out with the phase-stepping method [22]. Circumferential stress σ_θ was calculated using the generalized sum rule (25).

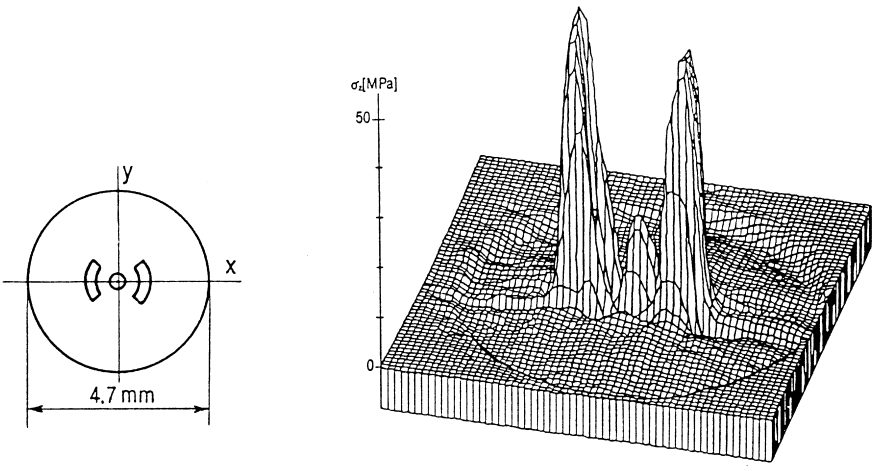

Fig. 9. Geometry of the cross-section of a bow-tie type optical fibre preform and axial stress distribution.

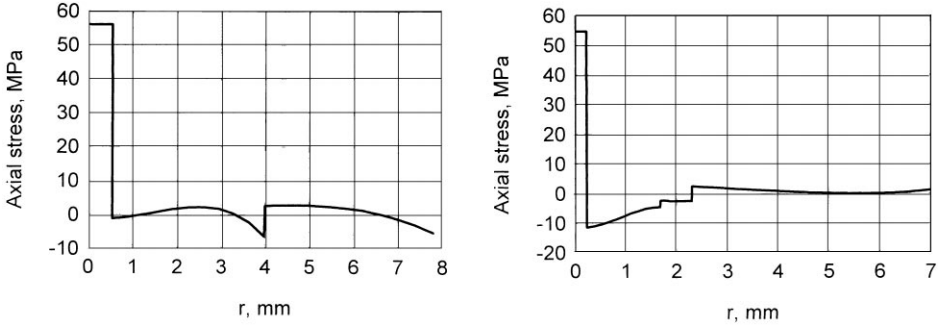

Fig. 10. Axial stress distribution in two step-index optical fibre preforms.

In Fig. 9, geometry of the cross-section of a bow-tie-type fibre preform and axial stress distribution are shown. In this case, tomographic photoelastic measurements were carried out for 60 azimuths and for every direction of the light beam the birefringence was recorded for 140 points. The other stress components can be calculated using a sophisticated algorithm [19].

Fig. 10 shows axial stress distribution in two step-index optical fibre preforms.

By investigating an axisymmetric glass article, the light can be passed through the latter perpendicular to different meridional sections (Fig. 11). In case of axisymmetric residual stress distribution, one should obtain with all measurements the same data (differing no more than the measurement errors), and interpretation of the data should give similar stress distribution all over the perimeter.

Practical measurement of residual stress in many bottles, tumblers, CRT neck tubes and other axisymmetric glass articles has shown that mostly that is not the case.

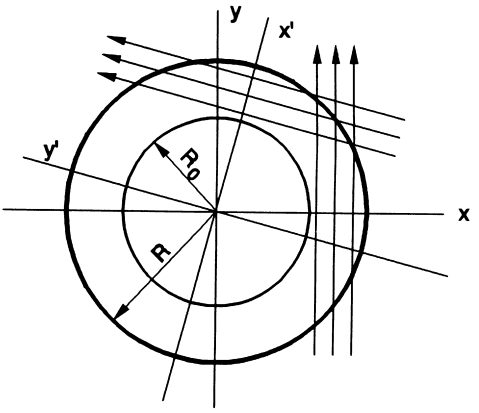

Fig. 11. At measurements the light can be passed through the axisymmetric article perpendicular to different meridional sections.

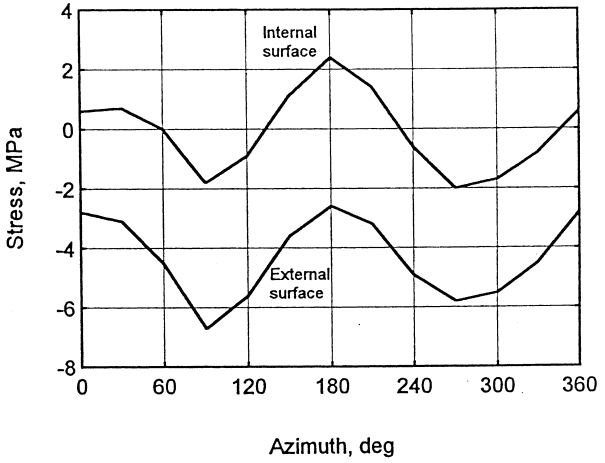

Fig. 12. Distribution of the meridional surface stress over the perimeter in the funnel of a CRT tube at 5 mm from the neck seal.

Almost always the residual stress distribution deviates from the axisymmetric one, often considerably. A method for measuring nonaxisymmetric stress distribution in axisymmetric glass articles has been developed [26]. As an example, Fig. 12 shows distribution of the axial stress over the perimeter on the surfaces of a CRT neck tube, 5 mm below the seal. Thus, photoelastic measurements should be carried out for various azimuths of the light beam in order to establish the real character of the stress distribution.

10. Conclusions

Integrated photoelasticity can be effectively used for automatic residual stress measurement and quality assessment of many glass products. At the same time, some theoretical problems related to nonlinear optical phenomena need further investigation in order to widen the scope of the method.

Acknowledgements

This paper was prepared in the course of research sponsored by the Estonian Science Foundation under grant No. 3595.

References

[1] Scholze H. Glass: nature, structure, and properties. New York: Springer, 1991.
[2] Jebsen-Marvedel H, Brückner R. editors Glastechnische Fabrikationsfehler. Berlin: Springer, 1980.
[3] Kuske A, Robertson G. Photoelastic stress analysis. London: Wiley, 1974.
[4] Aben H, Guillemet C. Photoelasticity of glass. Berlin: Springer, 1993.
[5] Augustsson BO, Wasylyk JS, Southwick RD. Computer modelled internal pressure strength predictions for refillable glass containers. Glastech Ber 1986;59(5):121–31.
[6] Müller-Simon H, Wagner J, Lenhart A. Practical strength of glass containers. Part 1: influence of the type of defect. Glass Sci Technol 1994;67(5):134–42.
[7] Crochet MJ, Denayer A. Transient and residual thermoviscoelastic stresses in glass. J Appl Mech 1980;47(2):254–60.
[8] Aben H. Integrated photoelasticity. New York: McGraw-Hill, 1979.
[9] Herman GT. Image reconstruction from projections. New York: Academic Press, 1980.
[10] Kak AC, Slaney M. Principles of computerized tomographic imaging. New York: IEEE Press, 1988.
[11] Aben H. Integrated photoelasticity as tensor field tomography. Proceedings of the International Symposium on Photoelasticity, Tokyo, 1986. Tokyo: Springer, 1986. p. 243–50.
[12] Aben H. Tomographie optique des champs de contraintes. Rev Franç Méc 1989;1:121–30.
[13] Doyle JF, Danyluk HT. Integrated photoelasticity for axisymmetric problems. Exp Mech 1978;18(6):215–20.
[14] O'Rourke RC. Three-dimensional photoelasticity. J Appl Phys 1951;22(7):872–8.
[15] Aben H, Ainola L, Anton J. Residual stress measurement in glass articles of complicated shape using integrated photoelasticity. Proceedings of the International Conference on Material Engineering, Gallipoli-Lecce, Vol. 1, 1996. p. 291–9.
[16] Aben H, Ainola L, Anton J. Sum rules for photoelastic residual stress measurement in axisymmetric glass articles. Proceedings of the International Conference on Advanced Technology in Experimental Mechanics (ATEM'99), Ube, Japan, Vol. 2, 1999. p. 629–34.
[17] Bartenev GM. The structure and properties of inorganic glasses. Groningen: Wolters-Nordhoff, 1970.
[18] Gardon R. Thermal tempering of glass. In: Uhlmann DR, Kreidl NJ, editors. Elasticity and strength of glass. Glass Science and Technology, Vol. 5. New York: Academic Press, 1980. p. 146–217.
[19] Puro AE, Kell K-JE. Complete determination of stress in fiber preforms of arbitrary cross-section. J Lightwave Technol 1992;10(8):1010–914.
[20] Aben H, Ainola L, Anton J. Complete residual stress measurement in axisymmetric glass articles. In: Allison IM, editor. Experimental mechanics, Vol. 2. Rotterdam: Balkema, 1998. p. 1343–6.
[21] Tomlinson RA, Patterson EA. Evaluating characteristic parameters in integrated photoelasticity. In: Allison IM, editor. Experimental mechanics, Vol. 1. Rotterdam: Balkema, 1998. p. 495–500.

[22] Aben H, Ainola L, Anton J. Half-fringe phase-stepping with separation of the principal stress directions. Proc Estonian Acad Sci Eng 1999;5(3):198–211.
[23] Anton J. Automatic measurement of residual stresses in tempered tumblers. Proceedings of the 18th International Congress on Glass, San Francisco, 1998;CD-ROM, A11. p. 9–13.
[24] Aben H, Josepson J. Strange interference blots in the interferometry of inhomogeneous birefringent objects. Appl Opt 1997;36(28):7172–9.
[25] Aben H, Ainola L. Interference blots and fringe dislocations in optics of twisted birefringent media. J Opt Soc Am 1998;A15(9):2404–11.
[26] Aben H, Anton J, Josepson J. Nonaxisymmetric residual stress distribution in axisymmetric glass articles. Glass Sci Technol 1996;69(3):75–81.